PERGAMON

Control Engineering Practice 8 (2000) 1023–1031

CONTROL ENGINEERING PRACTICE

www.elsevier.com/locate/conengprac

Maneuverability and smoke emission constraints in marine diesel propulsion☆

Anna Stefanopoulou[a,*], Roy Smith[b]

[a]Department of Mechanical & Environmental Engineering, University of California, Santa Barbara, CA 93106, USA
[b]Department of Electrical & Computer Engineering, University of California, Santa Barbara, CA 93106, USA

Received 22 April 1999; accepted 14 January 2000

Abstract

A multivariable control scheme is designed that reduces smoke generation on an experimental marine diesel engine equipped with a variable geometry turbocharger. The variable geometry turbocharger allows the improvement of the steady-state ship hydrodynamic and propulsion characteristics and requires coordination with the injected mass fuel to achieve a good transient performance.

Keywords: Marine propulsion; Multivariable control; Emissions

1. Introduction

Currently many international ports consider imposing stringent emissions requirements on recreational and commercial vessels. Specifically, in Frittz (1998) it is reported that the US Environmental Protection Agency (EPA) found that domestic and ocean-going marine diesel propulsion account for 4.5% of the total mobile source NO_x emission nationwide. The percentage contribution of NO_x and particulate matter (PM) emissions is much higher in port cities and coastal areas. Increased operational speeds reduce traveling time between ports, stressing the need for emission control during maneuvers in confined waters. The EPA and the International Maritime Organization (IMO) are in the process of proposing legislation requirements combining Tier 2 emission standards for Land-based Non-Road and Line-Haul Duty-Cycle Locomotive diesel engines with the Annex VI of the International Convention of Prevention of Pollution from Ships (MARPOL). It is anticipated that these new regulations will result in a 35% reduction of PM emissions which is associated with smoke generation during transient maneuvers.

In view of these new requirements, the shipping industry must develop technology to control emissions during ship transient maneuvers. Although, various innovative propulsion configurations which are not based on the internal combustion engine (Valenti, 1998) attempt to achieve this goal, the advantages of turbocharged diesel engines render them common practice for the vast majority of ocean freighters and offshore vehicles. In marine diesel propulsion, the turbocharger, the engine, and the propeller operation are optimized to achieve the rated power and maximum torque output. Thus, the turbocharger size is determined for high torque output which usually leads to large inertia and effective flow area and consequently slow air flow response. The slow air flow cannot match the required fast fueling commands during transient maneuvers and causes rich air-to-fuel ratio mixtures that result in high levels of visible smoke.

A mechanism that can potentially mitigate the inherent performance tradeoff between maximum power and transient emission performance is the variable geometry turbocharger. A turbine with variable geometry uses inlet guide vanes (v) on the turbine stator to modify its effective flow area as shown in Fig. 1. Changing the effective turbine flow area is advantageous. First, it provides a better match between the turbocharger and

* Corresponding author.
E-mail address: anna@engineering.ucsb.edu (A. Stefanopoulou).

☆Research supported in part by NSF under contracts ECS-97-33293; matching funds were provided by Turbodyne Inc. R. Smith supported by NSF under contract ECE-96-34498.

0967-0661/00/$ - see front matter
PII: S0967-0661(00)00024-1

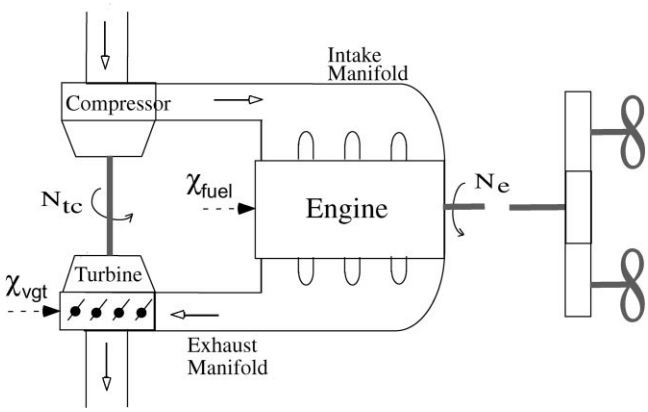

Fig. 1. Schematic representation of the VGT diesel engine.

the diesel engine in steady state (Moody, 1986). Secondly, it modifies the power transfer to the turbine and, hence, to the compressor which can potentially reduce the turbolag by speeding up the turbocharger response (Winterborne & Jai-In, 1991; Watson & Banisoleiman, 1988).

In this paper the feasibility and potential benefits of variable geometry turbocharger diesel engine for transient ship maneuvers and emission control are assessed. Several studies in automotive applications (see Kolmanovsky, Moraal, van Nieuwstadt & Stefanopoulou, 1997 and Stefanopoulou, Kolmanovsky & Freudenberg, 1998 for passenger vehicles and Winterborne & Jai-In, 1991 and Watson & Banisoleiman, 1988 for heavy commercial vehicles) have shown promising results. The intent here is to coordinate the injected fuel (W_f) and the variable geometry turbocharger (v) to jointly manage the fuel/air mixture into the cylinders. The multi-input multi-output (MIMO) controller is shown to improve torque and emission generation in marine diesel propulsion.

The MIMO controller is compared to the conventional diesel engine governor. Such a governor controls the combustion fuel supply during changes in load to maintain constant engine speed, and consequently, constant heading speed. Control algorithms that address the tradeoff between fuel economy and heading speed in the presence of wave induced disturbances are discussed in Hendricks, Holst, Poulsen and Joensen (1997) and Banning, Johnson and Grimble (1997). A comprehensive review of mechanical and electronic fuel governors can be found in Lilly (1984) and Haddad and Watson (1984). The actual injected fuel is restricted by the injection delays (Woodward & Latorre, 1984) and limiters that are employed to protect the shaft and prevent smoke. Smoke is generated during fast fueling transients by rich air-to-fuel ratio mixtures. Part of the energy in the combusted fuel is stored in the exhaust gas which is used by the turbocharger to spin up to a new steady-state operating point and eventually increase the amount of air to the engine. Thus, changes in fueling rate cause a disturbance in air-to-fuel ratio (ϕ) which is partially rejected through the natural feedback that the turbocharger establishes between the engine exhaust and intake processes. It takes, however, a certain amount of time for the turbocharger to spin up and for the intake manifold to fill to a new level of pressure and air mass, thus, reaching a new equilibrium. The slow dynamics in the engine air flow path causes a drop in the ϕ level which is associated with high hydrocarbon emissions and visible smoke generation. Any further drop in the ϕ level below the stoichiometric value affects the torque output as described in Woodward and Latorre (1984).

The variable geometry turbocharger provides an extra degree of freedom (i) to speed up the air loop dynamics, and consequently, reduce smoke generation without compromising the engine torque response and (ii) to improve steady-state ship speed. The controller must achieve satisfactory tradeoffs between conflicting goals such as maneuverability, fuel economy and emissions. Designing a model-based controller requires a low order and accurate representation of the engine and the propeller/surge dynamics. Section 3 describes the model for the turbocharger, engine, and surge dynamics. The steady-state optimization and plant linearization are presented in Sections 4 and 5. The control design and simulation results with projection on emission benefits are included in Sections 6 and 7. Finally in Section 8, air-to-fuel ratio estimation is discussed.

2. Nomenclature

The variables used in this paper are defined below. Other plant constants used in the mathematical model will be described in the text.

Variables

m	mass (kg)
W	flow rate (kg/s)
V	volume (m^3)
T	temperature (K)
Q	torque (Nm)
N	rot. speed (rpm)
P	power (W)
Ψ	force (N)
u	velocity (knots)

Super/subscripts

1	intake manifold
2	exhaust manifold
f	fuel
c	compressor
t	turbine
o	ambient
e	engine
p	propeller
r	resistance

3. Plant model

The variable geometry turbocharged diesel engine is described briefly with the following equations. The intake and exhaust manifolds are represented as finite volumes based on the "Filling and Emptying Methods" of plenum modeling described in Heywood (1988). The dynamic equations that characterize the manifold filling dynamics (Eqs. (1)–(4)) are based on the principles of conservation of mass, and the ideal gas law.

The two state equations for the intake manifold dynamics are given by:

$$\frac{\mathrm{d}}{\mathrm{d}t} m_1 = W_c - W_e, \tag{1}$$

$$\frac{\mathrm{d}}{\mathrm{d}t} p_1 = \frac{R}{V_1}(W_c T_o - W_e T_1). \tag{2}$$

Similarly, the two state equations for the exhaust manifold dynamics are given by:

$$\frac{\mathrm{d}}{\mathrm{d}t} m_2 = W_e + W_f - W_t, \tag{3}$$

$$\frac{\mathrm{d}}{\mathrm{d}t} p_2 = \frac{R}{V_2}((W_e + W_f)T_e - W_t T_2). \tag{4}$$

In the above, $R = c_p - c_v$. For simplicity, the same values of specific heats at constant pressure, c_p, and volume, c_v, are used for both intake and exhaust manifolds. In the above equations the heat transfer in the walls is neglected. This assumption is accurate for the intake manifold but it may not hold for the exhaust manifold due to the high exhaust temperature. The air into the intake manifold is assumed to be homogeneous. In addition to the above equations, the principle of conservation of momentum is also satisfied by assuming uniform pressure and temperature between the manifold restrictions.

The right-hand side of the above equations are determined using the engine and turbocharger manufacturer data. In particular, engine manufacturer data is used to describe (i) the engine volumetric efficiency, $\eta_v = f_{\eta_v}(p_1, T_1, p_2, T_2, N_e)$, and consequently, the engine mass air flow rate, W_e, (ii) the temperature rise between the engine intake and exhaust process, $\Delta T = T_e - T_1 = f_{\Delta T}(W_f, N_e, \phi, p_1)$, and (iii) the engine brake torque, $Q_e = f_{Q_e}(W_f, N_e, \phi, \eta_v ol)$ that is used in Eq. (6).

Acceleration of the turbocharger (Eq. (5)) and engine (Eq. (6)) is derived using Newton's second law.

The two state equations for the rotational dynamics are:

$$\frac{\mathrm{d}}{\mathrm{d}t} N_{tc} = \frac{P_t - P_c}{I_{tc} N_{tc}}, \tag{5}$$

$$\frac{\mathrm{d}}{\mathrm{d}t} N_e = \frac{Q_e - Q_p}{I_e + I_{add}}. \tag{6}$$

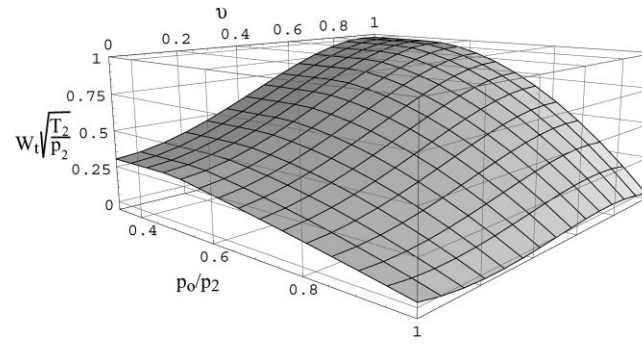

Fig. 2. Turbine mass flow parameter.

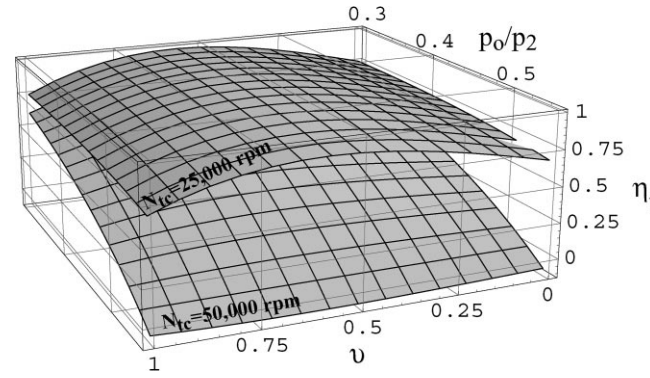

Fig. 3. Turbine efficiency.

In the above, I_{tc} and $I_e + I_{add}$ are the mass polar moment of inertia of the rotating systems. The turbine power and the compressor power, P_t and P_c, respectively, are calculated based on an ideal adiabatic process, and steady-state data provided by the turbocharger manufacturer. In particular, a "turbine map", f_t, is used to determine the turbine flow, W_t, and the efficiency, η_t, based on the pressure ratio between the upstream and the downstream turbine pressures, p_o/p_2, the turbocharger speed, N_{tc}, and the inlet guide vanes position, v:

$$\begin{bmatrix} W_t \\ \eta_t \end{bmatrix} = f_t\left(\frac{p_o}{p_2}, N_{tc}, v\right), \tag{7}$$

$$P_t = W_t c_p \eta_t \eta_m T_2 \left(1 - \left(\frac{p_o}{p_2}\right)^{(\gamma-1)/\gamma}\right). \tag{8}$$

The effect of the inlet guide vanes position, v, on the normalized turbine mass flow parameter, $W_t\sqrt{T_2/p_2}$, and the efficiency, η_t, is approximated by a third-order polynomial using least-squares fit (see Figs. 2 and 3).

Similarly, using data from the "compressor map" the compressor characteristics can be obtained:

$$\begin{bmatrix} W_c \\ \eta_c \end{bmatrix} = f_c\left(\frac{p_1}{p_o}, N_{tc}\right), \tag{9}$$

$$P_c = W_c c_p \frac{1}{\eta_c} T_o\left(\left(\frac{p_1}{p_o}\right)^{(\gamma-1)/\gamma} - 1\right). \tag{10}$$

Finally, the propeller torque, Q_p in Eq. (6), depends on the ship speed which is calculated based on Newton's first law.

The state equation for the surge dynamics is given by:

$$\frac{\mathrm{d}}{\mathrm{d}t} u = \frac{\Psi_p - \Psi_r}{m_\nabla + m_{hydro}}. \tag{11}$$

The ship displacement and the hull-wetted surface added virtual mass are denoted by $m_\nabla + m_{hydro}$ in the equation above. The propeller torque, Q_p, and thrust, Ψ_p, are determined using open water cavitation tank data supplied by the manufacturer, k_Q and k_Ψ, respectively, and are modified by hydrodynamic interactions between hull and propeller

$$Q_p = \rho N_p^2 D_p^5 k_Q(J), \tag{12}$$

$$\Psi_p = (1-t)\rho N_p^2 D_p^4 k_\Psi(J), \tag{13}$$

$$J = \frac{u(1-w)}{N_p D_p}, \tag{14}$$

where, w and t are the wake fraction and thrust deduction (assumed to be constant), and k_Q and k_Ψ are the wake and thrust coefficients (approximated by linear polynomials in the advance coefficient, J). The propeller speed, $N_p = N_e/gr$, is determined assuming a fixed gear ratio, and D_p is the propeller diameter.

3.1. Actuator dynamics

The actuator dynamics are modeled as first-order differential equations. The break frequency is defined by the stable and closed inner loop hydraulic controller:

$$\frac{\mathrm{d}}{\mathrm{d}t} W_f = \frac{1}{\tau_f}(\chi_{fuel} - W_f), \tag{15}$$

$$\frac{\mathrm{d}}{\mathrm{d}t} v = \frac{1}{\tau_v}(\chi_{vgt} - v). \tag{16}$$

The actuation signals, χ_{fuel} and χ_{vgt}, are generated by the control system, and the time constants, τ_f and τ_v, are approximately equal to 0.1 s.

Eqs. (1)–(6), (11), (15) and (16) constitute the nine states of the dynamic plant model, $[m_1, p_1, m_2, p_2, N_{tc}, N_e, u, W_f, v]$.

4. Steady-state optimization

The ship operator command usually involves a desired maneuver such as a sudden acceleration/deceleration or maintaining constant ship speed during wave-induced disturbances. The controller is designed to meet this operator command, while satisfying constraints in emissions and fuel economy. This objective imposes both steady state and transient requirements. The steady-state requirements of the control design goals is analyzed by studying the equilibrium points of the dynamic model discussed above. The model is simulated for a range of fueling levels, χ_{fuel}, and inlet guide vane positions, χ_{vgt}, and the achieved equilibriums are tabulated. Note here that for each pair of $(\chi_{fuel}, \chi_{vgt})$ values a unique equilibrium that is asymptotically stable is obtained. Fig. 4 shows the steady-state ship speed, u, engine speed, N_e, and air-to-fuel ratio, ϕ, plotted versus χ_{vgt} for different values of χ_{fuel}.

Firstly, for efficient marine propulsion it is desired to choose an inlet guide vane position that maximizes ship speed for a given constant fueling level. The χ_{vgt} values that achieve the maximum ship speed objective for each fueling level, from 5 to 13 kg/h, are shown with the dotted line in the upper subplot of Fig. 4. It is evident from the N_e-subplot of Fig. 4 that the steady-state engine speed and the steady-state ship speed are maximized for the same χ_{vgt} values.

Secondly, the emission constraints that are considered in this paper are related to smoke generation, and more generally, to hydrocarbon (HC) and particulate emissions. Large air-to-fuel ratios, ϕ, correlate with low hydrocarbon (HC) and particulate emissions. Hence, to reduce these type of emissions it is desired to choose χ_{vgt} that results in high air-to-fuel ratio, and in particular, an air-to-fuel ratio greater than 24 (limit for visible smoke generation). The χ_{vgt} values that achieve the maximum ϕ for each fueling level from 5 to 13 kg/h are connected with the dot-dash line in the lower subplot of Fig. 4.

Obviously the "maximum u" and "maximum ϕ" objectives cannot be satisfied simultaneously and the solid line (denoted by "selected setpoints" in Fig. 4) represents the χ^*_{vgt} values for which the best tradeoff between fuel economy and emissions is achieved for each fueling level. The "selected setpoints" line is also shown on the N_e-subplot in Fig. 4.

Using the above selected data and polynomial interpolation, a feedforward controller that calculates the desired steady-state engine speed, N^*_e, and air-to-fuel

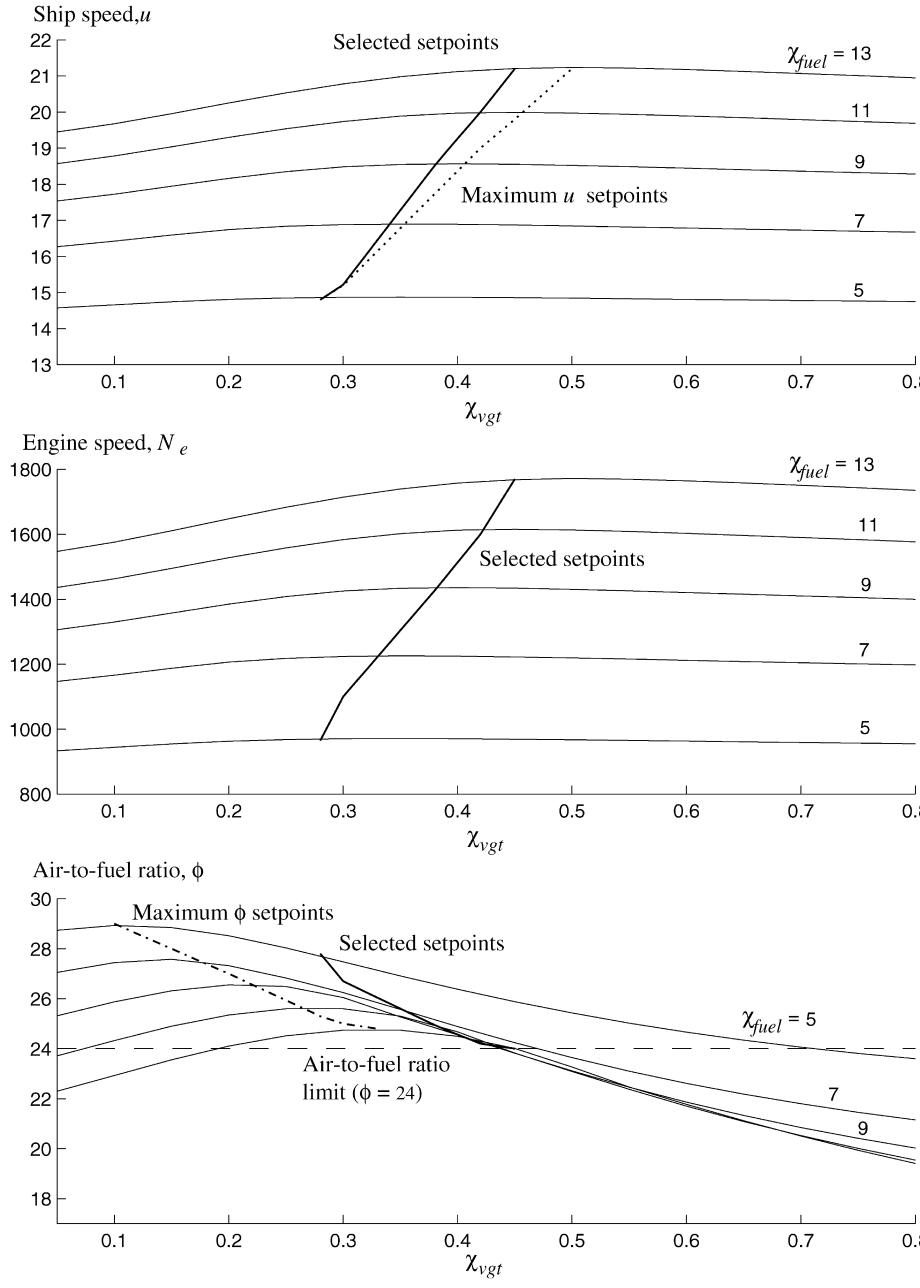

Fig. 4. Steady-state ship speed, u, engine speed, N_e, and air-to-fuel ratio, ϕ.

ratio, ϕ^*, based on the ship speed command, u^*, is derived. In Section 6 a linear multivariable feedback controller is designed that ensures tracking of the desired setpoints.

5. Dynamic open-loop characteristics

The frequency domain characteristics of the linearized plant are presented to better understand the interactions between the performance variables, N_e and ϕ, and the actuators, χ_{fuel} and χ_{vgt}. Linearization is performed at a nominal point, $\chi^*_{fuel} = 9.0$ kg/h, and $\chi^*_{vgt} = 0.38$. Bode magnitude plots in Fig. 5 describe the dynamic relation between the output scaled variables, $N_e/2000$ and $\phi/10$, and the scaled input variables, $\chi_{fuel}/10$ and χ_{vgt}. The scales are chosen based on range of values for each variable and relative importance in the control objectives. The dominance of the diagonal elements of the two-input two-output system at DC indicates, as expected, that χ_{fuel} strongly affects the steady-state value of N_e and χ_{vgt} strongly affects the steady-state value of ϕ.

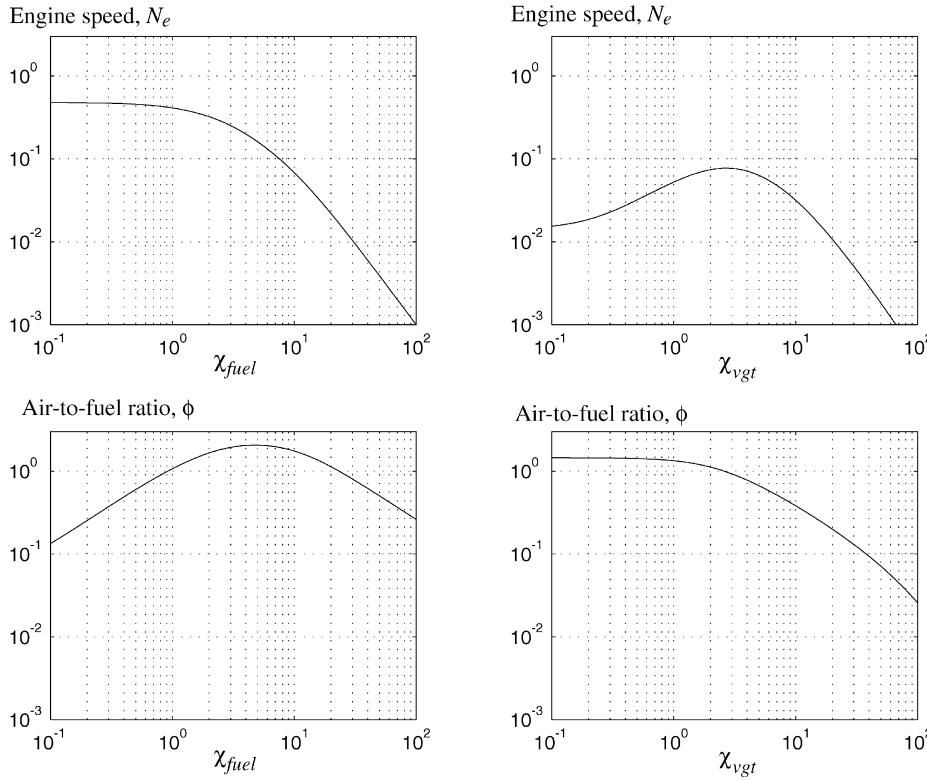

Fig. 5. Bode magnitude plots of the input, χ_{fuel} and χ_{vgt}, to the output, N_e and ϕ at a nominal operating point.

The effects of χ_{fuel} on N_e and ϕ illustrate the severe tradeoff between fast engine speed tracking and tight air-to-fuel ratio control in a conventional fixed geometry turbocharged diesel engine. Specifically, the peak of the interaction between χ_{fuel} and ϕ occurs at 5 rad/s and causes fast fuel commands to act as a disturbance to the ϕ subsystem. Therefore, to avoid undesirable disturbances of the air-to-fuel subsystem, the closed-loop fuel command must be designed to roll off before the frequency of interaction resulting in slow torque response. The variable geometry turbocharger, on the other hand, has enough authority to reject the disturbances that χ_{fuel} imposes to ϕ without significantly affecting N_e. Hence, a two-input two-output feedback control design can potentially enhance fast engine speed transients without degrading emission performance.

We note here that regulation or disturbance rejection in engine speed can successfully be used to regulate ship speed or maintain constant heading in rough seas. This argument is based on the similarity of the two speeds, u and N_e. In particular, ship speed exhibits slightly slower dynamics than the engine speed. In addition, engine speed is one of the easily measured variables, in contrast to ship speed, which renders it more suitable for control design.

On the other hand, finding an appropriate measurement for the air-to-fuel ratio regulation is not straight forward (van Nieuwstadt, Moraal & Kolmanovsky, 1998). For this reason, the feedback controllers are designed assuming that an accurate air-to-fuel ratio (ϕ) measurement is available. Then an air charge estimator based on an intake manifold pressure and temperature measurement is derived. The air charge estimator is used in the air-to-fuel ratio estimation and in the fuel limiter.

6. Control designs

Three control design strategies are compared on the above model. A measurement of the air-to-fuel ratio is assumed to be available. This allows the VGT-related control authority issues to be considered independently of any issues that would arise from the practical requirement of using only an estimate of the air-to-fuel ratio.

The first strategy uses a more standard proportional-integral (PI) design to control the engine speed, N_e, by actuating the fuel, χ_{fuel}. This has been tuned to give a good engine speed response to commanded engine speed step changes. Fig. 6 illustrates the configuration. Note that this does not allow the air-to-fuel ratio to be set independently of the engine speed since the inlet

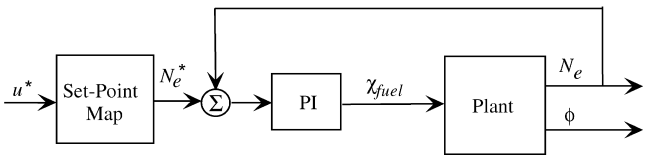

Fig. 6. PI configuration for engine speed control.

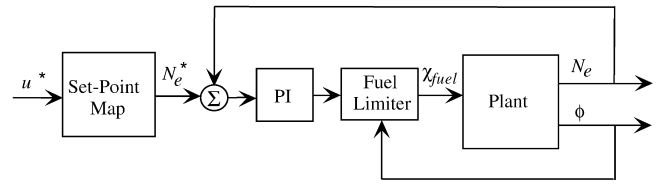

Fig. 7. PI with fuel limiter configuration for engine speed and air-to-fuel ratio transient control.

guide vanes are held fixed at 0.38. This configuration does not require the measurement (or estimation) of the air-to-fuel ratio.

It is known — and will be evident in the simulations presented — that this configuration can produce undesirable transients in the air-to-fuel ratio. The standard approach to alleviating this problem uses a fuel limiter when the air-to-fuel ratio drops below a specified value. This configuration is illustrated in Fig. 6. In the system discussed here the limiter adjusts the commanded fuel input to prevent the air-to-fuel ratio from dropping below $\phi = 24$. A measurement (or accurate estimation) of the air-to-fuel ratio is assumed. The PI controller now contains a standard anti-windup scheme to prevent the fuel limiter from causing controller-saturation-induced transients.

The design strategy for the variable geometry turbocharged engine (designated as MIMO in the subsequent analysis) uses measurements of both engine speed, N_e, and air-to-fuel ratio, ϕ, and is illustrated in Fig. 6. This allows tracking of both engine speed, N_e^*, and air-to-fuel ratio, ϕ^*. A weighted linear quadratic Gaussian (LQG) design, based on the linearized model, has been tuned for both transient performance and integral type (zero-steady-state error) tracking of N_e^* and ϕ^*. The relative weighting between the regulated variables and the actuators is the same as that used in the Bode plots in Fig. 5.

7. Simulation results

The above controllers have been evaluated on the nonlinear simulation model. The test maneuver involves a step change in ship speed from 18.6 to 21.2 knots. The set-point map generates a change in N_e^* from 1435 rpm to 1770 rpm, and a change in ϕ^* from 24.8 to 24.0. The closed-loop engine speed and air-to-fuel ratio responses are given in Fig. 7. The corresponding actuation signals are shown in Fig. 7.

The PI controller (dashed lines) gives the best engine speed response. This is achieved by a relatively fast change in fuel level which has the effect of producing a transient air-to-fuel ratio excursion which goes significantly below the excess smoke limit ($\psi = 24$).

As expected, the PI with fuel limiter (dot-dash lines) limits the rate of change of the fuel into the engine and prevents the air-to-fuel ratio from dropping below the smoke limit. However, it also has the effect of significantly degrading the engine speed response.

The MIMO controller (solid lines) gives an engine speed response which is close to that of the PI controller without creating a significant air-to-fuel ratio transient. This has been achieved by using the extra degree of freedom in the VGT actuation to control air-to-fuel ratio independently of the fuel flow rate. The VGT actuation is evident in Fig. 7.

Note also that the MIMO controller uses the VGT actuator to provide a different steady-state air-to-fuel ratio at the completion of the maneuver. The steady-state value of ϕ has been chosen as discussed in Section 4 and results in the same engine speed with less fuel; hence giving more efficient steady-state operation.

8. Closed-loop based on estimation

The fuel limiter and the MIMO controller in the above sections depend on accurate ϕ measurement. Although, ϕ sensors in diesel engines have been used in experimental work (Amstutz & Del Re, 1995), large delays, calibration requirements and high cost are important considerations for commercial applications. Hence, in this section a ϕ estimator is derived and connected to the previous closed-loop controllers. The air-to-fuel ratio estimator, $\hat{\phi}$, is based on an air charge estimator, $\hat{W}_e$, and the fuel command, χ_{fuel}:

$$\hat{\phi} = \frac{\hat{W}_e}{\chi_{fuel}}. \tag{17}$$

The air charge estimator, $\hat{W}_e$, is a static polynomial of intake manifold pressure and temperature measurements, p_1 and T_1, engine speed, N_e, and the control signals, χ_{fuel} and χ_{vgt}:

$$\hat{W}_e = \hat{W}_e(p_1, T_1, N_e, \chi_{fuel}, \chi_{vgt}). \tag{18}$$

The air charge estimator is a linear polynomial in all variables and all their possible linear combinations.

Connecting the air-to-fuel ratio estimator to the PI controller with the limiter and the MIMO controller

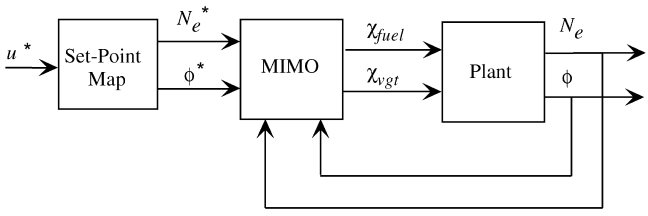

Fig. 8. MIMO configuration for engine speed and air-to-fuel ratio control.

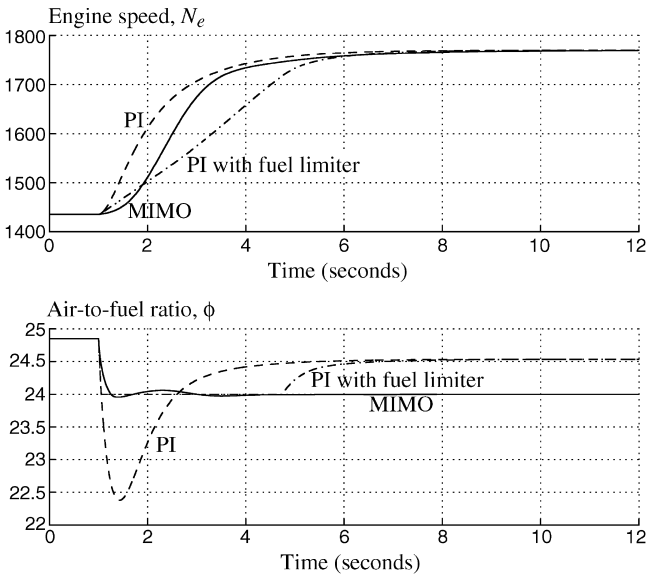

Fig. 9. Closed-loop step responses: PI (dashed), PI with fuel limit (dot–dash), and MIMO (solid) control systems.

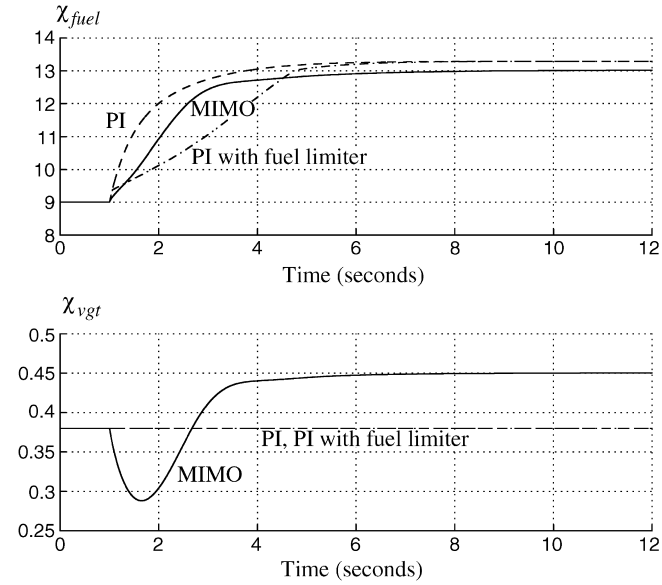

Fig. 10. Closed-loop actuation signals: PI (dashed), PI with fuel limit (dot–dash), and MIMO (solid) control systems.

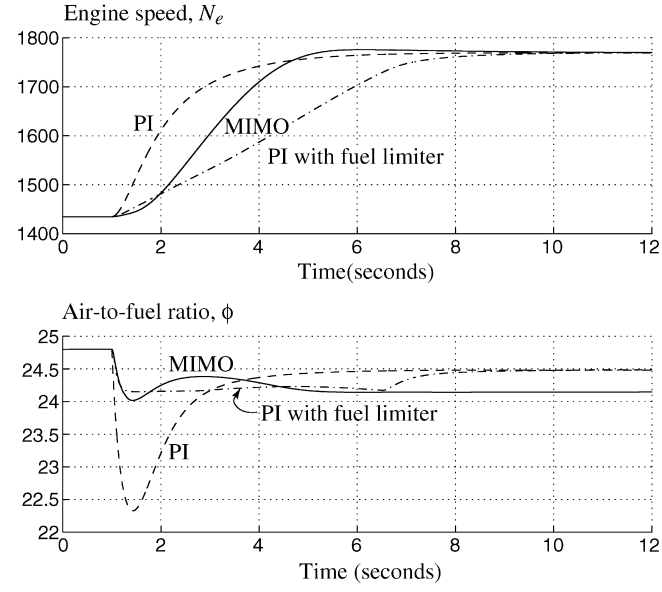

Fig. 11. Closed-loop step responses: PI (dashed), PI with fuel limit (dot–dash), and MIMO (solid) control systems.

described in Section 6 results in the closed-loop response shown in Fig. 8. The corresponding control signals are shown in Fig. 8. A small degradation is noticeable in the closed-loop performance of the two control schemes (compare Figs. 7 and 8) that use the estimated ϕ. The MIMO controller, again, outperforms the conventional (no VGT) PI controller with equivalent air-to-fuel ratio. The PI control scheme uses indirectly the estimated air-to-fuel ratio in the fuel limiter (Figs. 9–12).

Passenger cars with high-speed diesel engines utilize similar fuel limiters and are also based on steady-state feedforward estimation of air-to-fuel ratio (Guzzella & Amstutz, 1998). Although, the estimation algorithm performs well using only the steady-state information from engine mapping, future emission constraints will require the estimation of transient ϕ and a feedback configuration to reduce the sensitivity of the map parameters. Note that here the estimation of transient ϕ is more important in engines equipped with VGT than engines with conventional turbochargers. Controlling the variable geometry nozzles alters the exhaust manifold pressure dynamics, which consequently affects the engine volumetric efficiency, and thus, introduces a potentially large uncertainty in the steady-state air charge estimator. Recall here that during a load increase the optimal VGT trajectory has a non-minimum phase behavior; namely, VGT closes momentarily and eventually opens to a larger steady-state value (see Figs. 7 and 8). Robust and accurate estimation of transient air-to-fuel ratio will be the next stage of this work.

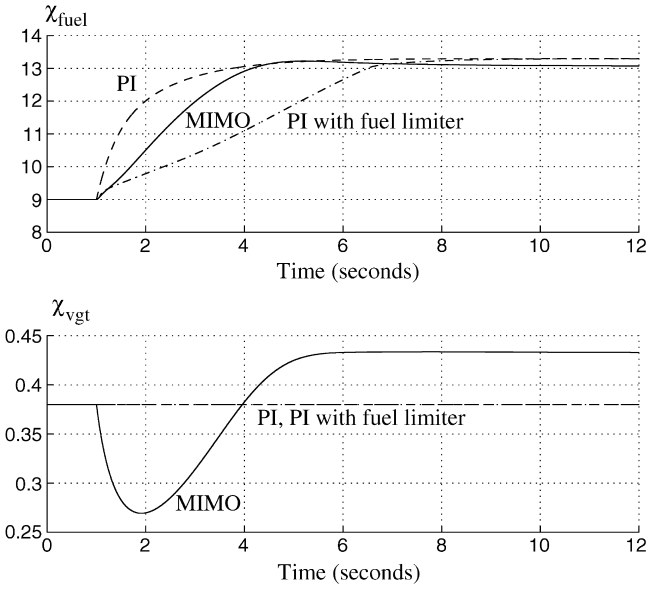

Fig. 12. Closed-loop actuation signals: PI (dashed), PI with fuel limit (dot–dash), and MIMO (solid) control systems.

9. Conclusions

The VGT gives an extra degree-of-freedom in the propulsion control system which allows some amount of independence between engine speed and air-to-fuel ratio. This gives significant performance advantages: in steady-state operation the air-to-fuel ratio can be tuned independently of engine speed to improve efficiency. In transient maneuvers the VGT can be used to prevent smoke producing transients in the air-to-fuel ratio without significantly degrading the engine speed response. Conventional approaches to this problem require a tradeoff between engine speed response and air-to-fuel ratio transient behavior. A MIMO controller must be used to take advantage of this additional capability. The results are based on linear analysis of the subsystem interactions at one operating point and evaluated using a nonlinear simulation. Experimental verification and detailed robustness analysis will be pursued in future work.

References

Amstutz, A., & Del Re, L. R. (1995). EGO sensor based robust output control of EGR in diesel engines. *IEEE Transactions on Control System Technology*, *3*(1), 39–48.

Banning, R., Johnson, M. A., & Grimble, M. J. (1997). Advanced control design for marine diesel engine propulsion. *ASME Journal of Dynamic Systems Measurements and Control*, *19*(2), 167–174.

Frittz, S. G. (1998). EPA setting exhaust regs. *ASME Internal Combustion Engine Division Newsletter*, 5–6.

Guzzella, L., & Amstutz, A. (1998). Control of diesel engines. *IEEE Control Systems Magazine*, *18*(2), 53–71.

Haddad, S., & Watson, N. (1984). *Principles and performance of diesel engineering*. Chichester: Ellis Horwood, 1984.

Hendricks, E., Holst, J., Poulsen, N.K., & Joensen, H. (1997). Adaptive minimum energy control of large ship Diesel Engine. *Proceedings of the Second IFAC Workshop on Adaptive Systems in Control and Signal Processing*, (pp. 231–236).

Heywood, J. B. (1988). *Internal Combustion Engine Fundamentals*. New York: McGraw-Hill.

Kolmanovsky, I., Moraal, P., van Nieuwstadt, M., & Stefanopoulou, A. (1997). Issues in modeling and control of intake flow in variable geometry turbocharged engines. In M. Polis, *Systems modeling and optimization* (pp. 436–445). London: Chapman Hall/CRC Research Notes in Mathematics.

Lilly, L. R. (1984). *Diesel engine reference book*. London: Butterworth.

Moody, J. F. (1986). Variable geometry turbocharging with electronic control. SAE paper No. 860107.

Stefanopoulou, A., Kolmanovsky, I., & Freudenberg, J. S. (1998). Control of variable geometry turbocharged diesel engine for reduced emissions. *Proceedings of the American control conference*, Philadelphia (pp. 1383–1388).

Winterborne, D. E., & Jai-In, S. (1991). The application of modern control theory to a turbocharged diesel engine powerplant. *Proceedings of the Institution of Mechanical Engineers Part I, Journal of Systems and Control Engineering*, *205*, 69–83.

Watson, N., & Banisoleiman, K. (1988). The variable-geometry turbocharger control system for high-output diesel engines. SAE paper No. 880118.

Woodward, J. B., & Latorre, R. G. (1984). Modeling of diesel engine transient behavior in marine propulsion analysis. *SNAME Transaction*, *92*, 33–49.

Valenti, M. (1998). Luxury liners go green. *Mechanical Engineering*, 72–73.

van Nieuwstadt, M., Moraal, P., & Kolmanovsky, I. (1998). Sensor selection for EGR–VGT control of a diesel engine. *Proceedings of AVCS'98, Advances in Vehicle Control and Safety*, Amiens, France (pp. 228–233).